

2010

# Experimental Determination of Flow and Heat Transfer Correlations for Passive Regenerators

Stefanie Marie Knauf

*University of Wisconsin-Madison*

Gregory Nellis

*University of Wisconsin-Madison*

Sanford Klein

*University of Wisconsin-Madison*

Follow this and additional works at: <http://docs.lib.purdue.edu/iracc>

---

Knauf, Stefanie Marie; Nellis, Gregory; and Klein, Sanford, "Experimental Determination of Flow and Heat Transfer Correlations for Passive Regenerators" (2010). *International Refrigeration and Air Conditioning Conference*. Paper 1038.  
<http://docs.lib.purdue.edu/iracc/1038>

This document has been made available through Purdue e-Pubs, a service of the Purdue University Libraries. Please contact [epubs@purdue.edu](mailto:epubs@purdue.edu) for additional information.

Complete proceedings may be acquired in print and on CD-ROM directly from the Ray W. Herrick Laboratories at <https://engineering.purdue.edu/Herrick/Events/orderlit.html>

## Experimental Determination of Flow and Heat Transfer Correlations for Passive Regenerators

Stefanie KNAUF\*, Gregory NELLIS, Sanford KLEIN

University of Wisconsin Department of Mechanical Engineering  
Madison, WI, United States

\*Corresponding Author: sknauf@wisc.edu

### ABSTRACT

Active Magnetic Regenerative Refrigeration (AMRR) systems are being considered as an environmentally friendly alternative to vapor compression refrigeration cycles. AMRR systems use solid refrigerants rather than a synthetic working fluid. With the use of an environmentally safe heat transfer fluid, such as water or a water propylene glycol solution, the ozone depletion potential and global warming potential for AMRR is essentially negligible. Further optimization of AMRR systems is required in order for them to become an economically attractive and viable substitute for current air conditioning and refrigeration units. Much of this optimization is focused on the regenerator matrix geometry and the thermal-fluid behavior of the packed bed of magnetocaloric material. As part of this effort, a passive single-blow test facility has been developed at the University of Wisconsin-Madison in order to measure the friction factor and the Nusselt number under conditions that are appropriate for AMRR systems.

### 1. INTRODUCTION

Recent increased interest in AMRR systems has led to the need for computer models that can accurately predict their behavior and performance in a computationally efficient manner. Engelbrecht (2005) developed a one-dimensional numerical model capable of predicting the performance of an AMRR system. However, comparison of the model with experimental measurements obtained from an AMRR prototype at Astronautics (Zimm *et al.*, 2006) showed that the model consistently over-predicted the performance of the system. This discrepancy is possibly a result of inaccurate calculation of the heat transfer and pressure drop associated with the regenerator. The one-dimensional numerical model utilizes correlations from the literature for the Nusselt number ( $Nu$ ) as a function of the Reynolds ( $Re$ ) and Prandtl ( $Pr$ ) numbers, and for the friction factor ( $f$ ) as a function of the Reynolds number. Frischmann (2009) designed and constructed a passive regenerator test bed that was installed in the single blow test facility. This regenerator is being used to verify existing correlations or, if necessary, develop a new correlation for the Nusselt number and/or friction factor in a bed of packed uniform spheres employing a liquid heat transfer fluid with a high Prandtl number.

#### 1.1 The Magnetocaloric Effect

Magnetic refrigeration is made possible by the magnetocaloric effect, which refers to the change in the entropy of a material due to magnetization. Understanding of the magnetocaloric effect is best achieved through an analogous comparison with the compression process for a common refrigerant used in vapor compression cycles. The fundamental property relation for a compressible substance is given by:

$$dU = T dS - P dV \quad (1)$$

A similar relation can be written for a magnetocaloric substance (provided that hysteresis is ignored):

$$dU = T dS + \mu_0 H d(VM) \quad (2)$$

Examination of equations (1) and (2) reveals that pressure ( $P$ ) is comparable to the applied magnetic field ( $\mu_0 H$ ) and the magnetic moment ( $VM$ ) is comparable to (the inverse of) volume ( $V$ ). When the compressible refrigerant is compressed adiabatically an increase in temperature will be induced; in an analogous process, an adiabatic magnetization of the magnetocaloric material causes an increase in its temperature. The next section discusses how the magnetocaloric effect may be used to produce refrigeration.

## 1.2 The AMRR Cycle

Figure 1 shows a simplified version of the AMRR cycle. During an AMRR cycle, a porous regenerator bed constructed from a magnetocaloric material is exposed to a time-varying magnetic field and a time-varying flow of heat transfer fluid.

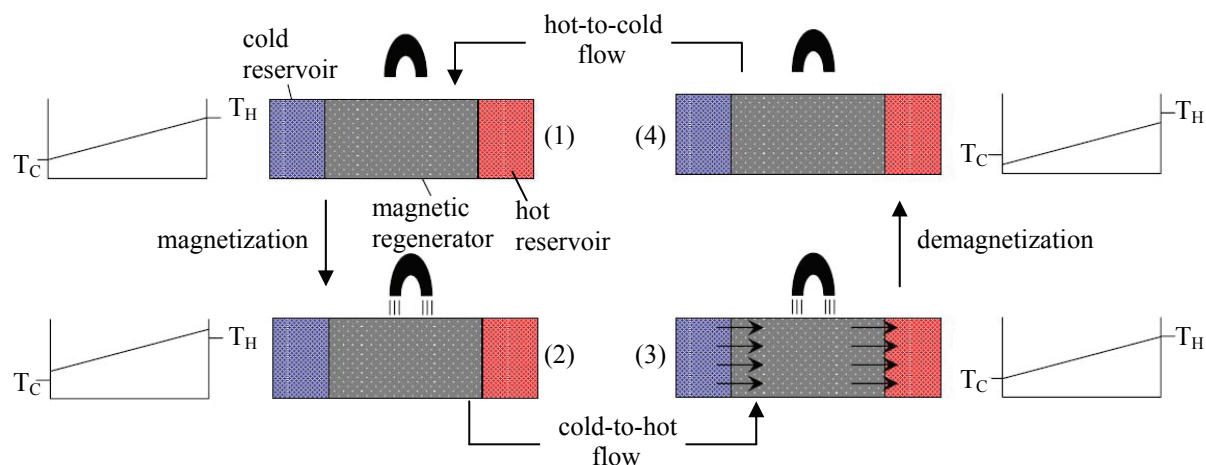


Figure 1: Active magnetic refrigeration cycle (Engelbrecht, 2005)

The process begins with the system at state (1) where the regenerator bed exhibits a temperature variation from the hot reservoir to the cold reservoir temperatures. The bed is magnetized causing it to transition from state (1) to state (2). There is no fluid flow during the magnetization process and therefore the temperature in the regenerator increases due to the magnetocaloric effect. The temperature distribution at state (2) (after magnetization) therefore results in temperatures that are higher than the hot temperature reservoir ( $T_H$ ) at the hot end. During the cold-to-hot-flow process, the heat transfer fluid flows through the bed from the cold reservoir to the hot reservoir. This flow of fluid from the cold reservoir causes the bed temperature to decrease, as shown in state (3). As a result of this process, fluid at a higher temperature than the hot reservoir is forced from the hot end of the bed causing a heat rejection. The bed is demagnetized causing it to transition from state (3) to state (4); this process results in a reduction in the temperature in the regenerator leading to the distribution shown in state (4). To get from state (4) back to state (1), heat transfer fluid is pushed back through the bed from the hot reservoir to the cold reservoir. The hot fluid brings the bed back to its original temperature profile and causes fluid at a temperature lower than the cold reservoir ( $T_C$ ) to flow from the cold end of the bed, resulting in a cooling effect.

## 2. UW AMRR SYSTEM MODEL

The UW AMRR model is a 1-D transient, numerical model that calculates the periodic steady state temperature of the regenerator material and the heat transfer fluid during a complete AMRR cycle (Engelbrecht, 2008). The model is explicit in time and implicit in space and is implemented using MATLAB. The model accepts water, a solution of propylene glycol and water or a solution of ethylene glycol and water as a heat transfer fluid which is assumed to be incompressible and therefore the density of the heat transfer fluid is constant. The remaining fluid properties are modeled as a function of temperature but not pressure. Hysteresis in the magnetocaloric material is neglected. The thermal conductivity of the magnetocaloric material is assumed to be a function of temperature and the entropy a function of temperature and applied field. Correlations from literature are used to calculate axial dispersion, Nusselt number, and local friction factor in the regenerator. A thorough description of the model is described by Engelbrecht (2008).

The UW AMRR model results have been compared to experimental data for a prototype AMRR utilizing a packed bed of spherical particles composed of commercial grade gadolinium (Gd). Figure 2 shows the predicted cooling power as a function of measured cooling power for these data. It is apparent from the figure that the UW AMRR model consistently over predicts the cooling power by, on average, approximately 20 W.

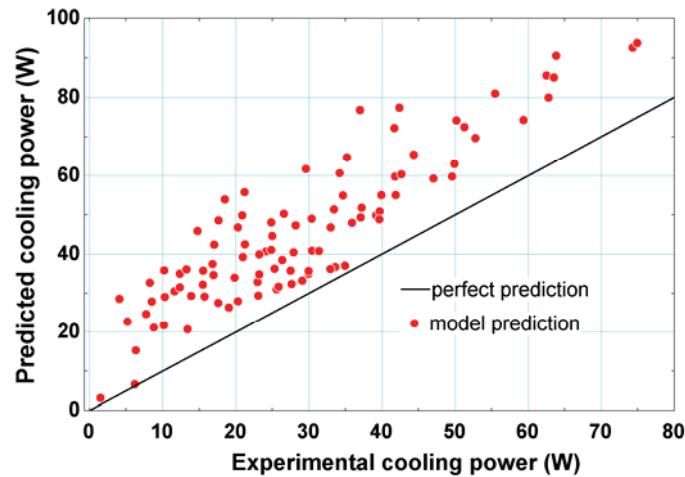


Figure 2: Predicted cooling power as a function of experimental cooling power (Engelbrecht, 2008)

One likely reason for the discrepancy shown in Figure 2 is that the Nusselt number or friction factor correlation used by the model is inaccurate or unsuitable for the range of Reynolds number ( $Re$ ) and Prandtl number ( $Pr$ ) that is used to produce the data (i.e., low Reynolds number and high Prandtl number). The Nusselt number is defined according to:

$$Nu = \frac{h d_p}{k_f} \quad (3)$$

where  $h$  is the heat transfer coefficient,  $d_p$  is the particle diameter and  $k_f$  is the thermal conductivity of the fluid. The friction factor is a function of the Reynolds number ( $Re$ ) and the Nusselt number is a function of both the Reynolds and Prandtl ( $Pr$ ) numbers as defined below.

$$Re = \frac{v_f d_p \rho_f}{\mu_f} \quad (4)$$

$$Pr = \frac{v_f}{\alpha_f} \quad (5)$$

where  $\rho_f$  is the density of the fluid,  $\mu_f$  is the viscosity of the fluid,  $v_f$  is the superficial velocity of the fluid as defined by the ratio of the volumetric flow rate of the fluid to the cross-sectional area of the test section,  $\nu_f$  is the kinematic viscosity of the fluid and  $\alpha_f$  is the thermal diffusivity of the fluid.

Several correlations exist for the Nusselt number inside a packed sphere regenerator. The UW AMRR model currently uses a correlation developed by Wakao and Kaguei (1982):

$$Nu_{Wakao} = 2 + 1.1 Re^{0.6} Pr^{1/3} \quad (6)$$

However, alternative correlations for the Nusselt number are provided by Kunii and Levenspiel (1969):

$$Nu_{Kunii} = 2 + 1.8 \left( \frac{Re}{\varepsilon_m} \right)^{1/2} Pr^{1/3} \quad (7)$$

and Macias – Mechin *et al.* (1991):

$$Nu_{Macias} = 1.27 + 2.66 \left( \frac{Re}{\varepsilon_m} \right)^{0.56} Pr^{-0.41} \left( \frac{1 - \varepsilon_m}{\varepsilon_m} \right)^{0.29} \quad (8)$$

Figure 3 shows the Nusselt number predictions for these three correlations for a Prandtl number of 30 and a bed porosity ( $\varepsilon_m$ ) of 0.36. The three correlations differ by a factor of approximately 5 under these conditions.



Obtaining measurements of Nusselt number is a more complex process that must be performed in two steps. The first step is to run the cold soak loop, indicated in Figure 4 by the bold, dashed line. During the cold soak, a continual flow of fluid is pumped through a heat exchanger where the fluid is cooled by flow from the cold temperature bath. The cold fluid leaving the heat exchanger passes through the regenerator; the cold soak loop is run until the test section is thermally stabilized at a uniform, low temperature. Immediately following the cold soak, a series of valves are switched so that the hot blow loop (bold solid line) is run through the test section producing a step change in fluid temperature driven by hot fluid extracted from the hot temperature bath. Temperature versus time data are gathered from the beginning of the temperature step change until a new thermal equilibrium is reached by the regenerator. The thermal behavior exhibited by the regenerator can be directly related to the fluid-to-matrix heat transfer, which allows the Nusselt number to be measured for a specific set of conditions. A detailed set of test facility operation instructions are given by Engelbrecht (2008).

#### 4. FRICTION FACTOR

The correlation developed by Ergun is the most widely used equation to describe pressure drop ( $\Delta p$ ) across a packed bed of spheres (Heggs, 2008):

$$\frac{\Delta p}{L} = c \frac{\mu_f v_f (1 - \varepsilon_m)^2}{d_p^2 \varepsilon_m^3} + m \frac{\rho_f v_f^2 (1 - \varepsilon_m)}{d_p \varepsilon_m^3} \quad (9)$$

where  $\varepsilon_m$  is the mean fractional void space of the packed bed (bed porosity),  $L$  is the length of the bed, and  $c$  and  $m$  are correlation constants obtained by fitting experimental data. Ergun's equation is the sum of two terms that correspond to viscous and inertial pressure loss. The friction factor can be defined by nondimensionalizing the pressure gradient by the viscous term (i.e., the first term) in order to obtain the viscous friction factor:

$$f_v = \frac{\Delta p}{L} \frac{d_p^2 \varepsilon_m^3}{\mu_f v_f (1 - \varepsilon_m)^2} = c + m \frac{Re}{(1 - \varepsilon_m)} \quad (10)$$

or by nondimensionalizing the pressure gradient by the inertial term, the second term in Eq. (9), in order to obtain the kinetic friction factor:

$$f_k = \frac{\Delta p}{L} \frac{d_p \varepsilon_m^3}{\rho_f v_f^2 (1 - \varepsilon_m)} = c \frac{(1 - \varepsilon_m)}{Re} + m \quad (11)$$

Ergun suggests values for  $c = 150$  and  $m = 1.75$ . Other correlations have the same form, but use slightly different constants. For example, MacDonald *et al.* use  $c = 180$  and  $m = 1.8$ . Both the Ergun and MacDonald correlations are compared to experimental data gathered using the passive regenerator test facility.

##### 4.1 Porosity

Porosity is defined as the ratio of the free volume to the total volume of the test section.

$$\varepsilon_m = \frac{V_F}{V_T} \quad (12)$$

Equations (10) and (11) show that the friction factor has a cubic dependence on porosity; consequently, even a small error in the measurement of the porosity can result in a substantial misrepresentation of the friction factor. Therefore, it is very important to obtain an accurate measurement of the porosity. The porosity can be measured using two different methods. The first method should be employed before the regenerator bed is assembled. The total volume of the test section is measured and the mass of the packing material is determined. Dividing the packing material mass by the density of the packing material provides the packing volume and dividing the packing volume by the total volume provides the fraction of the volume that is occupied by the spheres. Subtracting the packing fraction from unity provides the free volume fraction (i.e., the porosity) of the test section. The second method can be utilized after the regenerator test section is constructed. To determine the free volume, the test section is filled to capacity with water. The water is then poured from the regenerator into a graduated cylinder to determine the free volume. The free volume is divided by the total volume (determined before construction) in

order to obtain the porosity. The porosity for the regenerator used in the UW test facility was measured using both methods and found to be  $0.356 \pm 0.01$  and  $0.358 \pm 0.009$ , respectively. The two measurements are averaged, resulting in a porosity of 0.357.

#### 4.2 Experimental Setup

Pressure drop across the passive regenerator was measured using water at three different temperatures and a 30% propylene glycol and water solution at a single temperature. The three temperatures of water (26°C, 43°C, and 72°C) were specifically chosen to create a moderate change in viscosity and therefore in the Prandtl number (6.0, 4.1 and 2.6, respectively). The glycol solution was selected in order to provide a very large increase in viscosity and consequently in the Prandtl number (24.7). Such a large range of Prandtl numbers were used in order to verify that the Prandtl number of the fluid does not affect the friction factor/Reynolds number behavior. These same fluids are used during Nusselt number testing where the effect of Prandtl number is expected to be dramatic. Therefore, this verification is necessary in order to ensure that an observed effect of the Prandtl number on the Nusselt number is not an artifact of the experimental setup or procedure. For each run, flow rates were chosen to provide Reynolds numbers ranging from 1 to 225 so that a proper comparison could be achieved against Ergun and Macdonald friction factor correlations. Table 1 shows the flow rates corresponding to the Reynolds numbers for each run.

Table 1: Flow rates and corresponding Reynolds number

Reynolds Number	Flow Rate (L/min)			
	Water 26°C	Water 43°C	Water 72°C	30% PG 22°C
1				0.104
2				0.209
3	0.106			0.313
4				0.417
5	0.177	0.123		0.522
7	0.248	0.172	0.106	0.730
11	0.389	0.246	0.151	1.148
15	0.531	0.393	0.227	1.565
20	0.708	0.491	0.378	2.087
30	1.062	0.737	0.454	3.130
50	1.770	1.228	0.756	
70	2.478	1.719	1.059	
100	3.540	2.455	1.513	
140		3.438	2.118	
225			3.403	

A constant temperature bath was used to set the temperatures for the 43°C and 72°C runs. Two thermocouples at the top of the test section and two at the bottom of the test section are monitored and recorded during each test run. Data are collected starting at the highest flow rate and moving to the lowest flow rate. Data are then taken in the opposite order, beginning with the lowest flow rate and increasing to the highest flow rate, in order to ensure repeatability.

#### 4.3 Friction Factor Results

Figure 5 shows pressure drop as a function of volumetric flow rate for 43°C water data and 30% propylene glycol/water solution.

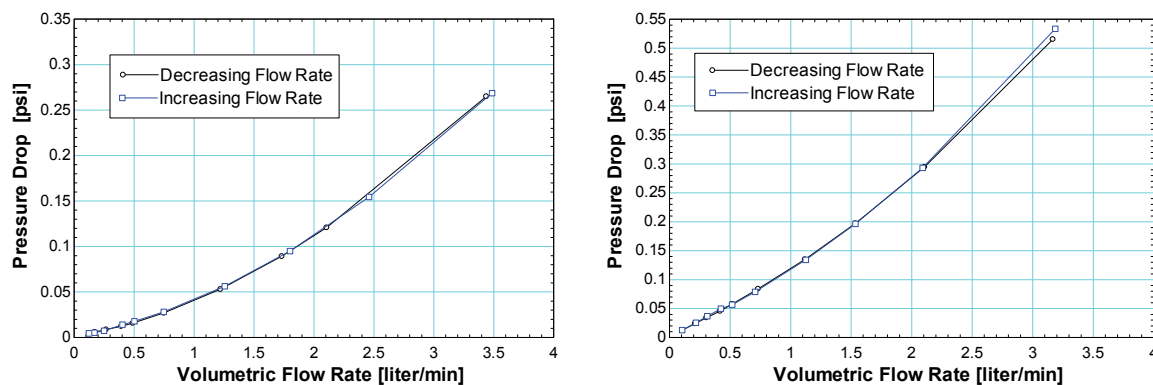


Figure 5: Pressure drop as a function of volumetric flow rate for 43°C water data (left) and 30% PG data (right)

The left-hand side of equations (10) and (11) are used to determine the friction factor from the collected pressure drop data. Figure 6 shows the friction factor (both viscous and kinetic) results with uncertainty bars for all four sets of data. Also shown in Figure 6 are the Ergun and Macdonald correlations.

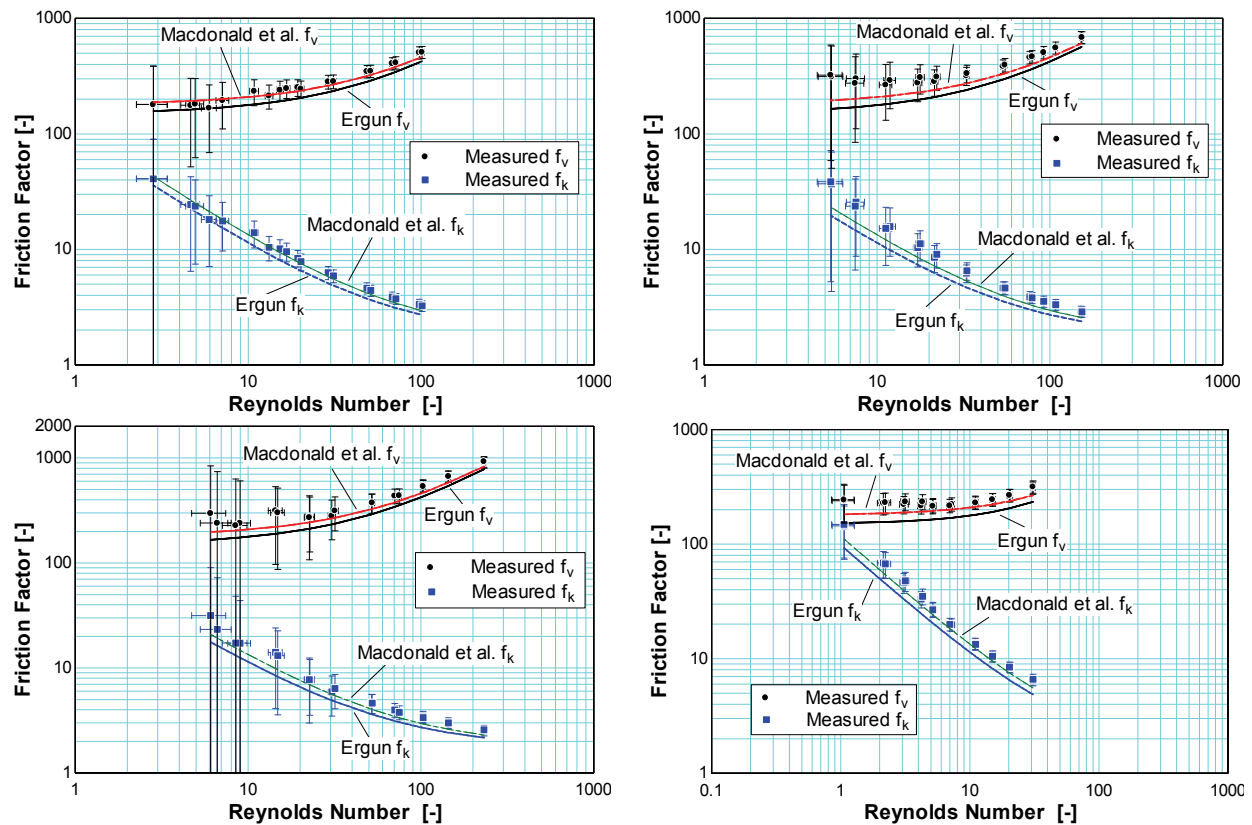


Figure 6: Friction factor as a function of Reynolds number for 26°C (upper left), 43°C (upper right), 72°C (lower left) water data and 30% PG data (lower right)

The uncertainty bars in Figure 6 are determined based on a complete uncertainty analysis for the experimental test facility. Table 2 shows a summary of the uncertainty values for a run at 1.12 L/min flow rate using 30% propylene glycol and water solution. As seen in the table, the major sources of uncertainty in the Reynolds number result from uncertainty in the fluid viscosity and fluid velocity. Uncertainty in the porosity accounts for about 62% of the uncertainty in the kinetic friction factor with the second largest contributor being uncertainty in the fluid velocity which accounts for 29% of the uncertainty.

Table 2: Summary of uncertainty values for 1.12 L/min flow rate for 30% PG solution

Variable	Description	Value	Variable	Description	Value
$\delta f_k$	Total uncertainty in the kinetic friction factor	1.202	$\delta Re$	Total uncertainty in the Reynolds number	0.506
$\delta f_{\Delta p}$	Uncertainty in the friction factor associated with pressure drop	0.356	$\delta Re_{\rho_f}$	Uncertainty in the Reynolds number associated with fluid density	$6.9 \times 10^{-3}$
$\delta f_{v_f}$	Uncertainty in the friction factor associated with fluid velocity	0.648	$\delta Re_{\mu_f}$	Uncertainty in the Reynolds number associated with fluid viscosity	0.430
$\delta f_{\varepsilon_m}$	Uncertainty in the friction factor associated with porosity	0.946	$\delta Re_{d_p}$	Uncertainty in the Reynolds number associated with particle diameter	0.045
$\delta f_L$	Uncertainty in the friction factor associated with length	0.022	$\delta Re_{v_f}$	Uncertainty in the Reynolds number associated with fluid velocity	0.263
$\delta f_{d_p}$	Uncertainty in the friction factor associated with the particle diameter	0.056			
$\delta f_{\rho_f}$	Uncertainty in the friction factor associated with the fluid density	$1.40 \times 10^{-6}$			

Figure 7 combines the viscous and kinetic friction factors from all three sets of water data as well as the 30% propylene glycol and water solution data. From Figure 7 it is concluded that the entirety of pressure drop data exhibits the most agreement with the Macdonald friction factor correlation.

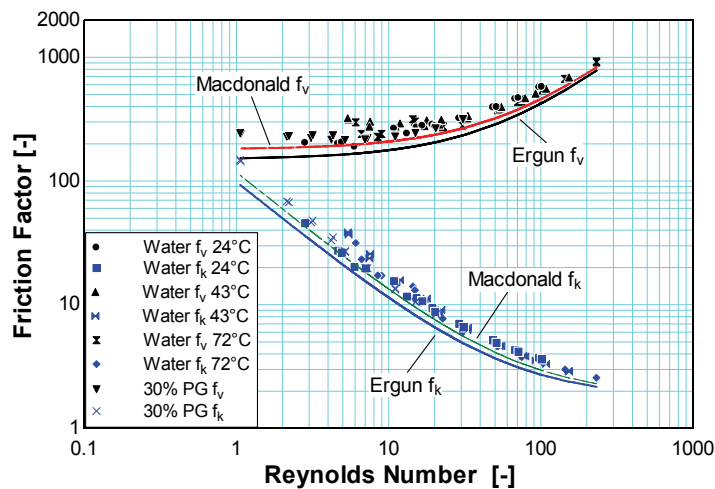


Figure 7: Friction factor as a function of Reynolds number for all four sets of pressure drop data

## 5. CONCLUSIONS

The friction factor data reveal that the pressure drop through the packed bed of uniform spheres is most closely represented by the Macdonald correlation. The uncertainty analysis of the data shows almost 100% agreement with the Macdonald correlation within the uncertainty band. The largest source of uncertainty in the friction factor is uncertainty in the porosity of the packed bed and therefore a meticulous measurement of this parameter is necessary in order to obtain accurate data. Future work will focus on experimental measurement of the Nusselt number for uniform spheres as well as other geometries such as packed beds of non-uniform diameter spheres, non-spherical particles, and connected matrices.

## REFERENCES

- Engelbrecht, K., 2008, *A Numerical Model of an Active Magnetic Regenerator Refrigerator with Experimental Validation*, M.S. Thesis, University of Wisconsin Madison.
- Engelbrecht, K., 2005, *A Numerical Model of an Active Magnetic Regenerator Refrigeration System*, M.S. Thesis, University of Wisconsin Madison.
- Frischmann, M., 2009, *Heat Transfer Coefficient Using Liquid Heat Transfer Fluids for use in Active Magnetic Regenerative Refrigeration*, M.S. Thesis, University of Wisconsin Madison.
- Heggs, P.J., 2008, Fixed Beds, In: Hewitt, G.F., *Heat Exchanger Design Handbook 2008*, vol. 2, Begell House, New York: p. 2.2.5-1-25-7.
- Kunii, D., Levenspiel, O., 1969, *Fluidization Engineering*, Wiley, New York, NY, 534.
- Macias-Machin, A., Oufar, L., Wannenmacher, N., 1991, Heat Transfer between an Immersed Wire and a Liquid Fluidized Bed, *Powder Technology*, vol. 66:281-284.
- Marconnet, A., 2007, *Predicting Regenerator Performance with a Single-Blow Experiment*, M.S. Thesis, University of Wisconsin Madison.
- Wakao, N., Kaguei, S., 1982, *Heat and Mass Transfer in Packed Beds*, Gordon and Breach Science Publishers, New York, NY, 364.
- Zimm, C., Boeder, A., Chell, J., Sternberg, A., Fujita, A., Fujieda, S., Fukamichi, K., 2006, Design and Performance of a Permanent Magnet Rotary Refrigerator, *International Journal of Refrigeration*, vol. 29, 8:1302-1306.

## ACKNOWLEDGEMENT

The authors gratefully acknowledge the support from Astronautics for this research. In particular, Steve Jacobs, Carl Zimm, and Andre Boeder have provided valuable discussions and technical input.